

Electrophoretic Deposition and Characterization of Highly Exothermic Al/CuO Nanothermites

Miao He¹, Yuting Xie¹, Zihui Ni¹, Xuzhong Zeng¹, Hebin Bao², Xiaodi Wu³, Li Liu³, Xueming Li^{1,*}, Qihui Wang^{1,3,*}

¹ School of Chemistry and Chemical Engineering, Chongqing University, Chongqing 400044, China

² Army logistical University of PLA, Chongqing 401311, China

³ Institute for Health and Environment, Chongqing University of Science and Technology, Chongqing 401331, China

*E-mail: lxm301@cqu.edu.cn (Xueming Li), qihuiwang@cqu.edu.cn (Qihui Wang)

Received: 9 September 2020 / Accepted: 31 October 2020 / Published: 30 November 2020

Based on the superior exothermic properties, Al/CuO nanothermites are considered as one of the most promising energetic materials in recent years. In this work, the CuO nanospheres with particle size of 100–120 nm were successfully synthesized by a simple solution route and subsequent heat treatment, and used as oxidizer of Al/CuO nanothermites. The electrophoretic deposition kinetics of Al/CuO nanothermites were investigated in detail. Then, the morphology and composition of the as-prepared Al/CuO nanothermites were characterized by means of scanning electron microscopy (SEM), X-ray diffraction (XRD), X-ray photoelectron spectroscopy (XPS), and spectrophotometry. The results show that the electrophoretic deposition behavior of Al/CuO nanothermites is controlled by diffusion. Furthermore, there is a linear relationship between the equivalent ratio in the suspension (Φ_d) and the deposited film (Φ_s). The Φ_d can be precisely adjusted by changing the electrophoresis parameters. When the equivalent ratio of Al/CuO nanothermites in the suspension is 1.5, the heat release of the sample can reach up to 1977 J/g. This work provides a new strategy for the preparation of nanothermites by electrophoretic deposition.

Keywords: Al/CuO; Thermites; Electrophoretic deposition; Exothermic properties

1. INTRODUCTION

As a kind of composite energetic material, thermite plays an important role in defense industry and economic construction due to its high energy density, oxygen carrying capacity and quality density[1-7]. However, with the fast development and great progress of society, the performance of traditional thermite cannot meet the stricter requirements in practical applications due to its high onset reaction temperature, poor exothermic performance and slow combustion rate[8-20]. Therefore,

exploring new thermites with excellent reaction performance has become a hot topic in the field of energetic materials. Usually, nano sized fuel and oxidizers can effectively shorten the mass transfer distance between components and significantly improve their exothermic and combustion performance, which can greatly improve the reaction performance of thermites[21-24].

Copper oxide (CuO) has been widely applied as oxidizer in thermite due to its low cost and abundant reserve[25-33]. Meanwhile, when the thermal reaction occurs, a remarkable amount of heat can be released, causing the newly formed Cu to quickly evaporate into Cu vapor. As a result, the volume of the reaction system expands rapidly, resulting in a violent explosion. Therefore, Al/CuO nanothermites have become one of the hotspots in the research of energetic materials in recent years.

In this study, the kinetics of electrophoretic deposition process of Al/CuO nanothermites on Ti electrodes was investigated in detail. The structure and chemical composition of Al/CuO nanothermites sample were systematically characterized by SEM, XRD, XPS and spectrophotometry. Finally, the exothermic behavior of the sample was evaluated by DSC.

2. EXPERIMENTAL SECTION

2.1 Materials

Aluminum nanoparticles (Al, 100 nm), polyethyleneimine (PEI, Mw=10,000), ammonia ($\text{NH}_3 \cdot \text{H}_2\text{O}$) and ascorbic acid ($\text{C}_6\text{H}_8\text{O}_6$) were purchased from Aladdin Industrial Corporation (Shanghai, China). Copper sulfate ($\text{CuSO}_4 \cdot 5\text{H}_2\text{O}$), sodium hydroxide (NaOH), isopropanol ($\text{CH}_3\text{CHOHCH}_3$) and glucose ($\text{C}_6\text{H}_{12}\text{O}_6 \cdot \text{H}_2\text{O}$) were purchased from Kelong Industrial Inc. (Chengdu, China). All chemical reagents were of analytical grade and utilized without any further purification.

2.2 Preparation of CuO nanospheres

According to our previous study[20], CuO nanospheres were obtained via a facile solution route at room temperature and followed by a calcination process. Firstly, $\text{CuSO}_4 \cdot 5\text{H}_2\text{O}$ (1.88 g) and glucose (10.00 g) were dissolved in 50 mL of deionized water for 30 min through magnetic stirring at room temperature. Subsequently, 125 mL of $\text{NH}_3 \cdot \text{H}_2\text{O}$ (0.04 mol/L) and 125 mL of NaOH (0.20 mol/L) were added into the above mixed solution. After stirring for 30 min, 250 mL of ascorbic acid (0.03 mol/L) was quickly added to the reaction system. The reaction continued for 1 h to obtain final precipitates. The precipitates were collected by centrifugation, washed several times with deionized water and ethanol, and dried in an electric oven at 400 °C for 2 h.

2.3 Synthesis of Al/CuO nanothermites

In this work, the Al/CuO nanothermites were prepared via electrophoretic deposition (EPD) process. Firstly, the Ti electrodes with a size of 8.00 cm × 1.50 cm × 0.06 cm were polished with abrasive paper from grade 400# to 1000# to remove the oxide layer. After that, the Ti electrodes were thoroughly

rinsed with deionized water and ethanol several times and dried naturally. Next, solid thermite particles (CuO nanospheres and Al nanoparticles) with a total mass of 0.10 g were added into 100 mL isopropanol to prepare 1.00 g/L suspension by ultrasonic dispersion. The additive (PEI) with 2.5 wt.% was also added. After ultrasonic treatment, the Ti electrodes were quickly inserted into the above suspension, and the distance between the two electrodes was adjusted to 1.00 cm. The EPD process was carried out at a voltage of 100 V and a deposition time of 10 min. Finally, after the EPD process, the Ti electrode with solid particles was taken out and dried in a vacuum oven at 80 °C for 2 h.

Before preparing Al/CuO nanothermites, the effect of additive (PEI) content on deposited mass was explored. The EPD dynamics was carried out under different field strengths and deposition time with 2.5 wt.% of PEI. During the kinetics study, the variation curve of current density was recorded. The mass change of the Ti electrode before and after the deposition process were also recorded.

2.4 Characterization

The composition and morphology of CuO nanospheres and Al/CuO nanothermites were characterized by X-ray diffraction (XRD) and scanning electron microscopy (SEM). The elemental composition of Al/CuO nanothermites were characterized by X-ray photoelectron spectroscopy (XPS). In addition, the exothermic properties of Al/CuO nanothermites were measured by differential scanning calorimetry (DSC).

Besides, the mass percentage of CuO nanospheres in the Al/CuO nanothermite was determined by spectrophotometry to realize the controllable preparation of Al/CuO nanothermites. The method is verified by contrasting the determined copper content with the actual copper content in the Copper sulfate.

3. RESULTS AND DISCUSSION

3.1 The EPD behavior of Al/CuO nanothermites

In this experiment, it was observed that the deposited mass of CuO nanospheres on the Ti electrode increased significantly with the addition of PEI. Therefore, PEI was used as additive for EPD process. Firstly, the deposited mass of CuO nanospheres on the Ti electrode was investigated, with the PEI amount ranging from 0 wt.% to 20 wt.%. As can be clearly seen in Figure 1, when the PEI content is 2.5 wt.%, the deposition mass of CuO nanospheres on the Ti electrode has a significant deposition amount. With the further increase of PEI content, the deposition quantity of CuO nanospheres did not improve significantly. Therefore, PEI with a content of 2.5 wt.% was applied in the further EPD process of Al/CuO nanothermites.

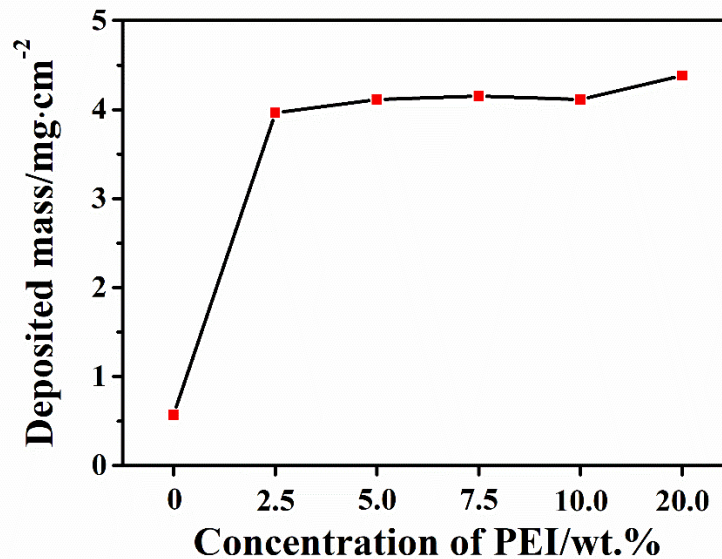


Figure 1. Relationship between deposition mass and PEI concentration in electrophoresis CuO nanospheres under a voltage of 100 V and a deposition time of 10 min.

As displayed in Figure 2, the current density–deposition time curves under different field strengths were recorded in detail. Figure 2 (a) shows that the variation curve of current density with deposition time in the deposition process of Al/CuO nanothermites under three different voltage of 100 V, 150 V and 200 V. The current density decreases gradually with the increase of deposition time. In the EPD process, the solid particles in the suspension are deposited on the Ti electrode and precipitated by gravity[34-37]. As a result, the concentration of particles in the suspension decreases, causing the current density to gradually decrease as the deposition time increases. Furthermore, under a certain field strength, the thickness of the deposited film increases gradually. The current flowing through the electrode decreases according to Ohm's law.

Figure 2 (b) exhibits the relationship between the current density and the square root of deposition time under three different field strengths of 100 V, 150 V and 200 V. The results show a good linear relationship between the current density and the square root of the deposition time, indicating that the EPD behavior of Al/CuO nanothermites conforms to the Cottrell equation shown in formula (1). Therefore, the electrophoretic deposition process can be considered to be controlled by diffusion[27, 38-40].

$$i = k c \sqrt{\frac{D_0}{\pi t}} \quad (1)$$

where i is the current density, k is the constant, D_0 is the coefficient of diffusion, t is the deposition time.

The mass of the Ti electrode before and after EPD process was accurately weighed by precision balance, and the deposition mass and deposition time curve of Al/CuO nanothermites under three different field strengths of 100 V, 150 V and 200 V were obtained. As shown in Figure 2 (c), the deposition mass of the sample increases linearly with the increase of the field strength. Moreover, it can be observed from Figure 2 (d) that the deposition mass of Al/CuO nanothermites showed a trend of

gradual increase with the increase of deposition time. Figure 2 (d) shows the relationship between deposition mass and deposition time under different field strengths. The deposition mass increases with the increase of deposition time, which can be fitted as $m=a\sqrt{t}+b$, and the functional relationship are as follows:

$$\textcircled{1} 100 \text{ V} \quad m=2.51304\sqrt{t} - 1.51347 \quad R^2=0.99299 \quad (2)$$

$$\textcircled{2} 150 \text{ V} \quad m=2.40735\sqrt{t} - 0.78006 \quad R^2=0.98197 \quad (3)$$

$$\textcircled{3} 200 \text{ V} \quad m=2.85357\sqrt{t} - 0.60050 \quad R^2=0.99172 \quad (4)$$

where m is the mass of Al/CuO nanothermites per unit area (mg/cm^2), and t is the deposition time (min). These results indicate that the deposition process of Al/CuO nanothermites is mainly controlled by diffusion.

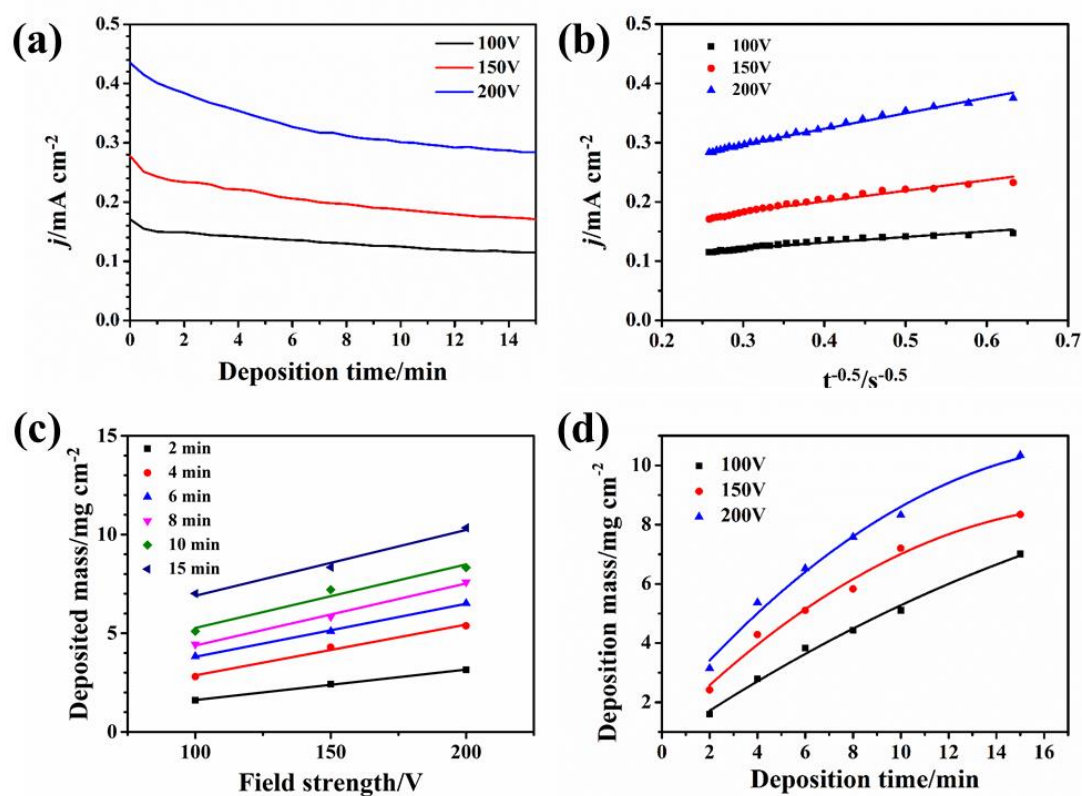


Figure 2. (a) Current density–deposition time curves for three field strengths of 100 V, 150 V and 200 V, (b) Changes of current density with $t^{-0.5}$ under different field strengths in EPD process of Al/CuO nanothermites, (c) The relationship curves between the deposition mass of Al/CuO nanothermites and the field strength at different deposition times, (d) Deposited mass of Al/CuO nanothermites as a function of deposition time under different field strengths.

3.2 Characteristics of Al/CuO nanothermites

The structure and morphology of the samples were investigated by SEM. As shown in Figure 3 (a), the as-prepared CuO nanospheres are highly homogeneous with a regular size of 100~120 nm. From the Figure 3 (b), the average diameter of the Al nanoparticles is about 60~100 nm. Figure 3 (c)

shows the SEM of Al/CuO nanothermites prepared by EPD. The Al nanoparticles and CuO nanospheres are uniformly distributed. Furthermore, as shown in Figure 3 (d), corresponding elemental mapping of Al/CuO nanothermites proves the uniform distribution of Al, Cu, and O elements. The signal of C element signal comes from the PEI used in the EPD process. Especially, the presence of porphyritic Al element signals in the elemental mapping is caused by the aggregations of Al particles.

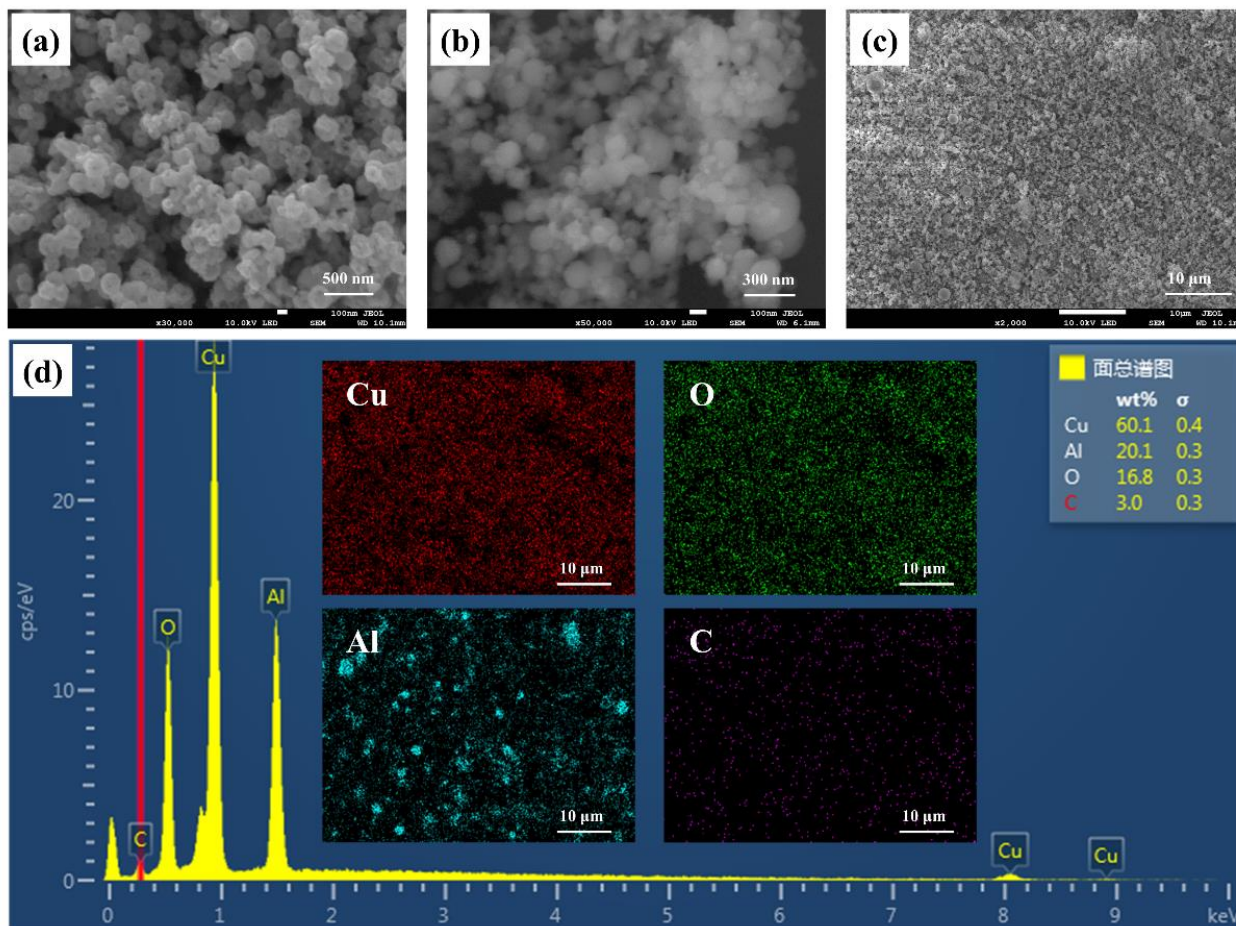


Figure 3. The SEM images of (a) CuO nanospheres, (b) Al nanoparticles and (c) deposited Al/CuO nanothermites. (d) the corresponding elemental mapping of Al/CuO nanothermites.

The phase composition of the as-prepared Al/CuO nanothermites was characterized employing XRD analysis. Figure 4 shows the XRD pattern of Al/CuO nanothermites prepared by electrophoretic deposition. The predominant peaks observed in the samples at 32.48° , 35.38° , 38.47° , 38.64° , 44.72° , 48.85° , 53.35° , 58.16° , 61.51° , 65.09° , 65.66° , 66.34° , 66.51° , 67.72° , 68.01° , 72.33° , 74.86° , 78.22° , 82.43° and 83.69° correspond to standard diffraction pattern of Al (JCPDS No. 89-4037) and CuO (JCPDS No. 80-0076). Besides, no diffraction peaks other than Al and CuO are observed in Figure 4, indicating that the Al/CuO nanothermites prepared by EPD are composed of pure Al and CuO. Moreover, there was no reaction between Al nanoparticles and CuO nanospheres during the EPD process.

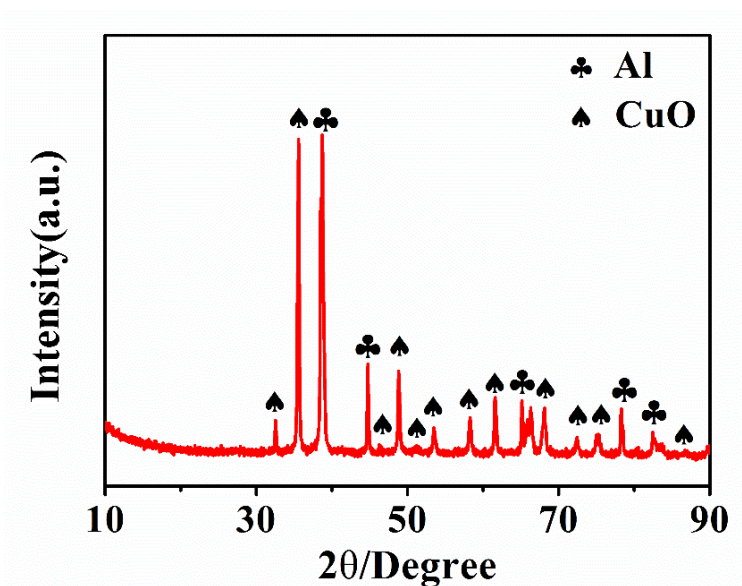


Figure 4. XRD pattern of Al/CuO nanothermites prepared by electrophoretic deposition.

Determination of copper content can be conducted by many methods, such as inductively coupled plasma mass spectrometry (ICP-MS)[41], flame atomic absorption spectrometry[42] and anodic stripping voltammetry[43] and so on. Here, the proportion of CuO nanospheres in Al/CuO nanothermites was determined a facile and precise method, spectrophotometry. As shown in Figure 5, the Cu^{2+} content (C) has a good linear relationship with absorbance (A) in the range of 3–24 mg, the correlation coefficient $R^2=0.99961$, and the regression equation is: $A=0.02908C+0.001$.

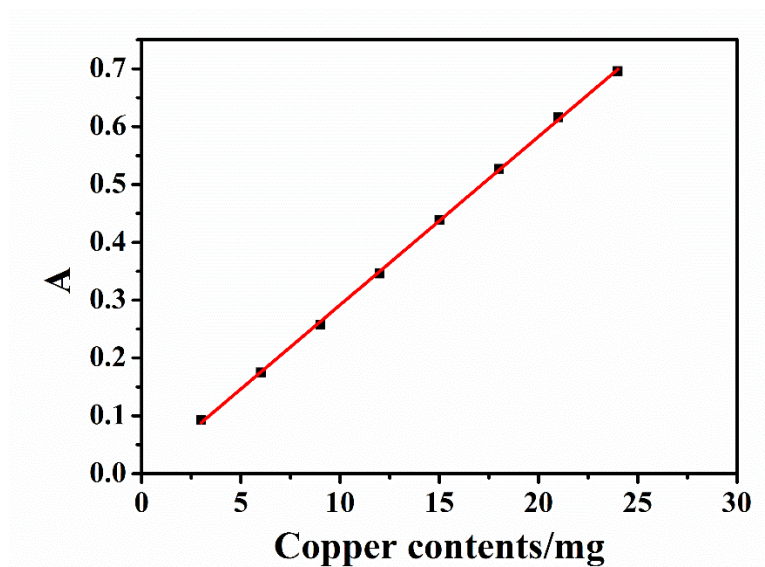


Figure 5. Standard curve for determination of copper content.

The relative error between the actual copper content and the measured copper content was further verified by spectrophotometry. As shown in Table 1, the relative error between the actual value and

measured value of copper content is less than 2.00%, and the average error is 1.46%. Therefore, the results show that spectrophotometry can be applied to determine the equivalent ratio by measuring the CuO content in Al/CuO nanothermites. Nuket Kartal Temel and Ramazan Gürkan also presented a method for determination of trace Cu(II) by spectrophotometry, showing good sensitivity and ease of operating[44].

Table 1. The comparison of the actual value with the measured value of samples' copper content

Serial number	Measured copper content /mg	Actual copper content /mg	relative error
1	10.8	10.6	1.85%
2	13.5	13.3	1.48%
3	15.6	15.3	1.92%
4	18.6	18.4	1.08%
5	20.4	20.2	0.98%

Due to the different sedimentation and migration rates of Al and CuO in the suspension[26], the equivalent ratio of Al/CuO nanothermites in the suspension (Φ_s) is quite different from the equivalent ratio of Al/CuO nanothermites deposited on the Ti electrode (Φ_d). The Φ_d of the Al/CuO nanothermites was determined by spectrophotometry. As shown in Figure 6, there is a good linear relationship between Φ_d and Φ_s . The linear regression equation is: $\Phi_d = 0.43171\Phi_s + 0.11925$ ($R^2=0.98394$). Therefore, the Φ_d can be precisely controlled by adjusting the Φ_s to meet the requirements of different application scenarios.

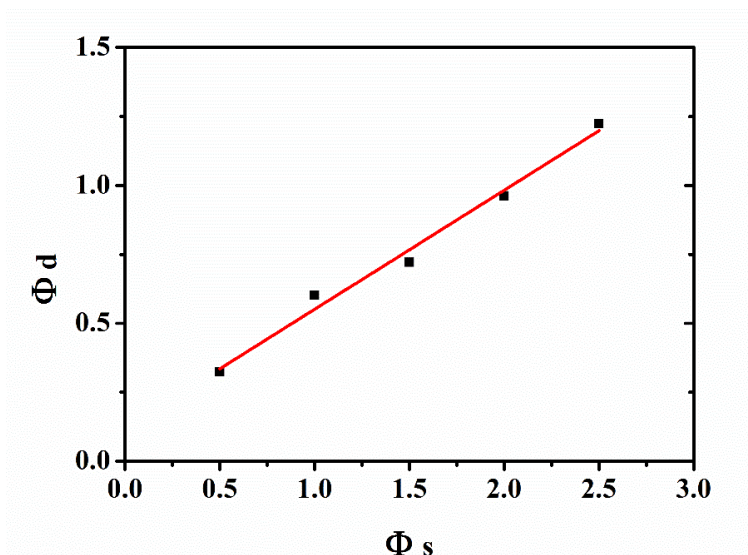


Figure 6. The relationship between equivalence ratio of Al/CuO nanothermites (Φ_d) and that in suspension (Φ_s).

The surface elements and chemical states of as-prepared Al/CuO nanothermites were characterized by XPS. The XPS spectra of the as-prepared samples were shown in Figure 7. In Figure 7

(a), the binding energy of 76 eV, 285 eV, 399 eV and 530 eV correlates to the Al 2p, C 1s, N 1s and O 1s, respectively. The peak ranging from 933~960 eV represents the Cu 2p. The results show that the sample contains Cu, Al, C, N and O element. Figure 7 (b–f) shows the high resolution spectra of Al 2p, Cu 2p, O 1s, C 1s and N 1s. In Figure 7 (b), the peak at 76 eV derive from 2p of Al, indicating that Al element exists in the form of elemental substance in sample. As observed in Figure 7 (c), the peaks at 932.8 eV and 952.6 eV are attributed to 2p 3/2 and 2p 1/2 of Cu.

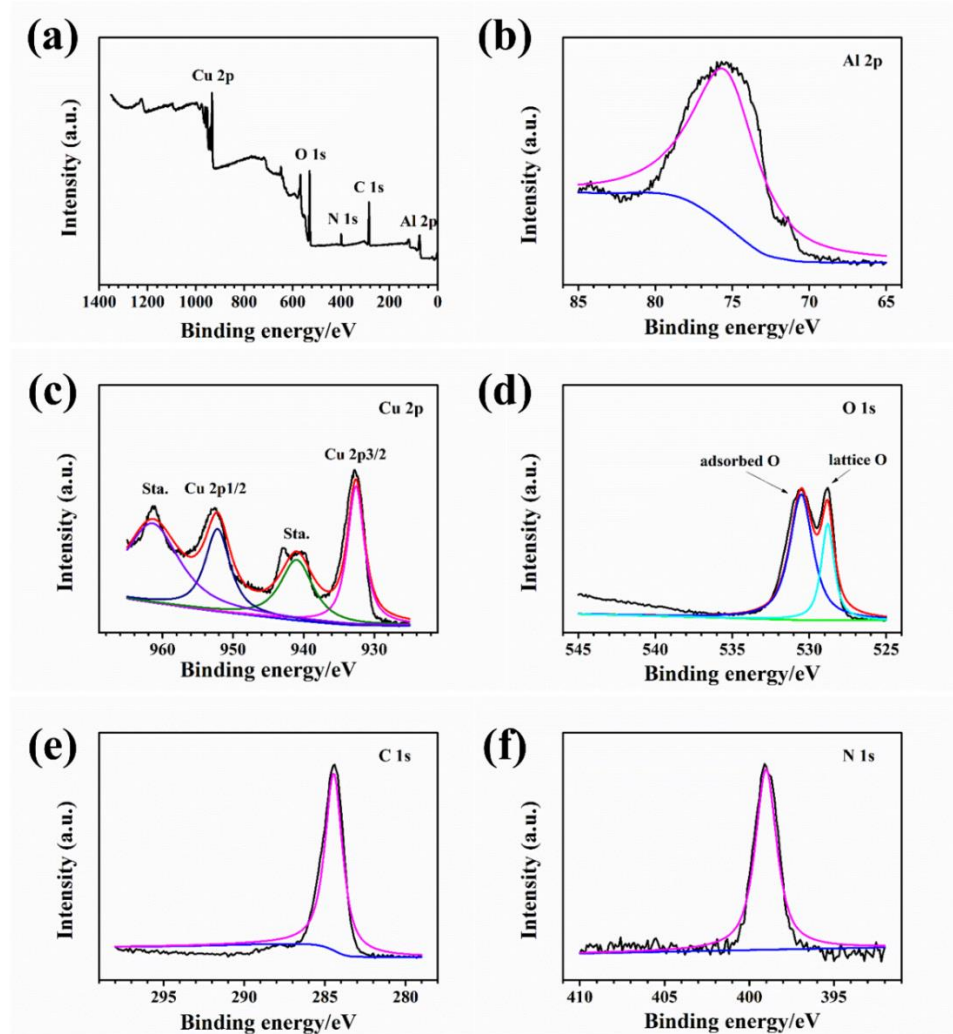


Figure 7. XPS spectra of (a) Al/CuO nanothermites, high resolution XPS spectra of (b) Al 2p, (c) Cu 2p, (d) O 1s, (e) c 1s and (f) N 1s.

Meanwhile, there are also two satellite peaks at 942.8 eV and 961.4 eV, confirming that the oxide in the sample is CuO. It can be seen from Figure 7 (d) that the binding energy peaks of O 1s at 528.8 eV and 530.5 eV correspond to lattice oxygen and adsorbed oxygen in CuO, respectively. The peak at 285 eV in Figure 7 (e) corresponds to the peak of C 1s, which originates from the C–C bond in PEI. In Figure 7 (f), the peaks of C (399 eV) derive from the C–N bond of PEI. The above XPS analysis results verify that the components of the samples are Al and CuO. In addition, the presence of PEI used in the EPD process is also demonstrated.

3.3 Exothermic behavior of Al/CuO nanothermites

The exothermic behavior of Al/CuO nanothermites were investigated by DSC. The DSC test was carried out in a 99.999% Ar atmosphere. The heating range was from room temperature to 1000 °C, and the heating rate was 20 °C/min. Figure 8 shows the DSC curves of Al/CuO nanothermites with different equivalence ratio. It is observed in Figure 8 (a–e) that the onset reaction temperature of all nanothermites with different equivalent ratios are about 340 °C. In these samples, the first sharp exothermic peaks appear at about 595 °C, corresponding to the solid–solid reaction between solid Al nanoparticles and CuO nanospheres. The weak endothermic peak at 655 °C corresponds to the melting of the Al nanoparticles. The second exothermic peaks appear at about 775 °C, corresponding to the solid–liquid reaction between melted Al and solid CuO.

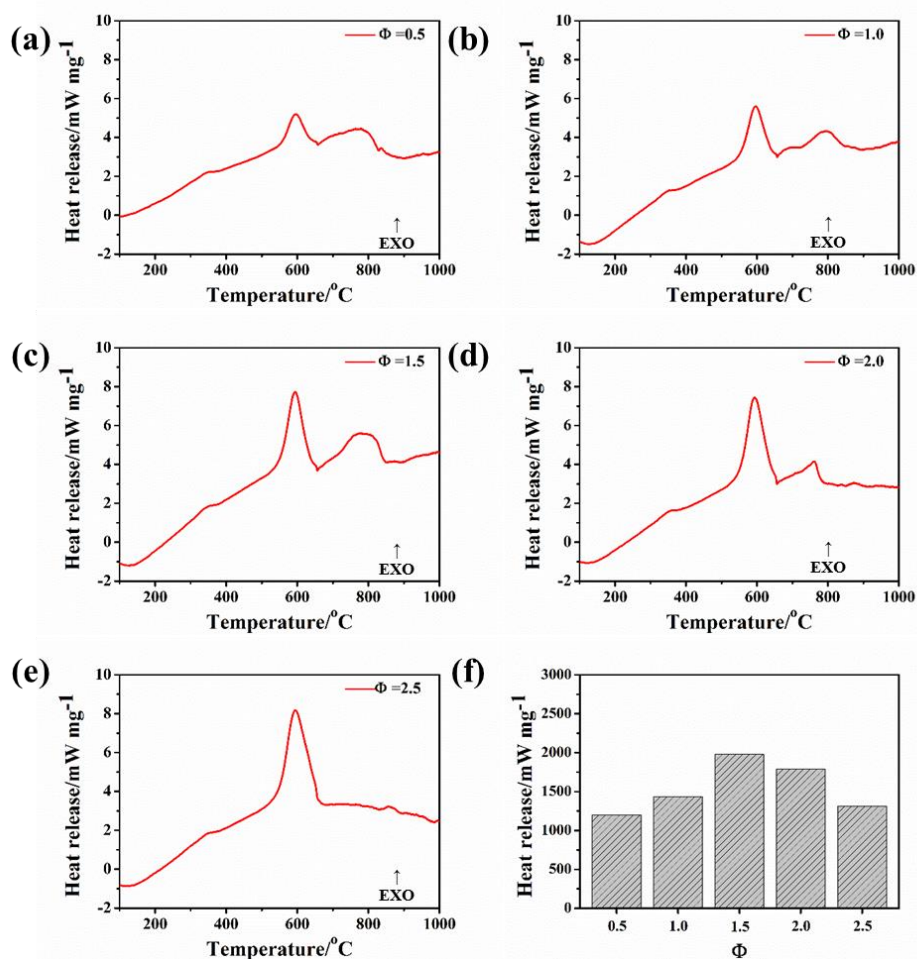


Figure 8. The DSC curve of Al/CuO nanothermites with different equivalence ratios: (a) $\Phi_s=0.5$, (b) $\Phi_s=1.0$, (c) $\Phi_s=1.5$, (d) $\Phi_s=2.0$, (e) $\Phi_s=2.5$. (f) the relationship between the heat release and the equivalent ratio of Al/CuO nanothermites.

The heat release of Al/CuO nanothermites with different equivalence ratio was calculated by the software attached to DSC. The heat released by the Al/CuO nanothermites is shown in Figure 8 (f), which are 1200 J/g ($\Phi_s = 0.5$), 1433 J/g ($\Phi_s = 1.0$), 1977 J/g ($\Phi_s = 1.5$), 1791 J/g ($\Phi_s = 2.0$) and 1313 J/g ($\Phi_s = 2.5$), respectively. When Φ_s is 1.5, Al/CuO nanothermite exhibits the best heat release.

4. CONCLUSIONS

The CuO nanospheres with a particle length of 100~120 nm were successfully synthesized by a facile solution route and subsequent heat treatment, and used as oxidizer for nanothermites. The Al/CuO nanothermites were prepared by electrophoretic deposition method. It was found that the electrophoretic deposition kinetics of Al/CuO nanothermites was controlled by diffusion. The results show that the equivalent ratio of Al/CuO nanothermites in suspension (Φ_d) is linearly related to the equivalent ratio on the Ti electrode (Φ_s), and the Φ_d can be adjusted precisely by changing the electrophoretic deposition parameters. When Φ_s is 1.5, the heat release of Al/CuO nanothermites can reach 1977 J/g. This work provides a new strategy for the preparation of nanothermites using electrophoretic deposition technology.

References

1. J.X. Song, X. Fang, T. Guo, F.L. Bei, W. Ding, X.N. Zhang, M. Yao and H.J. Yu, *J. Brazil Chem. Soc.*, 29 (2018) 404.
2. M.R. Weismiller, J.Y. Malchi, R.A. Yetter and T.J. Foley, *P. Combust. Inst.*, 32 (2009) 1895.
3. G. Jian, L. Liu and M.R. Zachariah, *Adv. Funct. Mater.*, 23 (2013) 1341.
4. C. Yu, W. Zhang, R. Shen, X. Xu, J. Cheng, J. Ye, Z. Qin and Y. Chao, *Mater. Design*, 110 (2016) 304.
5. M. Wang, L. Qiu, X. Zhao, Y. Li, T. Rao, S. He, L. Qin and J. Tao, *Mater. Sci. Eng., A*, 757 (2019) 23.
6. A.A.L. Michalchuk, M. Trestman, S. Rudic, P. Portius, P.T. Fincham, C.R. Pulham and C.A. Morrison, *J. Mater. Chem. A*, 7 (2019) 19539.
7. K.J. Kim, M.H. Cho, J.H. Kim and S.H. Kim, *Combust. Flame*, 198 (2018) 169.
8. N. Wang, Y. Hu, X. Ke, L. Xiao, X. Zhou, S. Peng, G. Hao and W. Jiang, *Chem. Eng. J.*, 379 (2020) 122330.
9. Y. Mao, L. Zhong, X. Zhou, D. Zheng, X. Zhang, T. Duan, F. Nie, B. Gao and D. Wang, *Adv. Eng. Mater.*, 21 (2019) 1900825.
10. J. Song, T. Guo, M. Yao, J. Chen, W. Ding, F. Bei, Y. Mao, Z. Yu, J. Huang, X. Zhang, Q. Yin and S. Wang, *Vacuum*, 176 (2020) 109339.
11. X. Mei, G. Zhong and Y. Cheng, *J. Energetic Mater.*, 37 (2019) 378.
12. B. Hu, W. Zhang, C. Yu, Z. Zheng, Y. Chen, J. Wang, J. Liu, K. Ma and W. Ren, *Ind. Eng. Chem. Res.*, 58 (2019) 7131.
13. S. Knapp, N. Eisenreich, S. Kelzenberg, E. Roth and V. Weiser, *Propell. Explos. Pyrot.*, 44 (2019) 706.
14. A. Nicollet, L. Salvagnac, V. Baijot, A. Esteve and C. Rossi, *Sensor. Actuat. A-Phys.*, 273 (2018) 249.
15. C.P. Yu, W.C. Zhang, B. Hu, D.B. Ni, Z.L. Zheng, J.P. Liu, K.F. Mai and W. Ren, *Nanotechnology*, 29 (2018) 36LT02.
16. F. Saceleanu, M. Idir, N. Chaumeix and J.Z. Wen, *Front. Chem.*, 6 (2018) 10.
17. X. Ke, X. Zhou, H. Gao, G. Hao, L. Xiao, T. Chen, J. Liu and W. Jiang, *Mater. Design*, 140 (2018) 179.
18. J. Dai, F. Wang, C. Ru, J. Xu, C. Wang, W. Zhang, Y. Ye and R. Shen, *J. Phys. Chem. C*, 122 (2018) 10240.
19. Z. Zheng, W. Zhang, C. Yu, G. Zheng, K. Ma, Z. Qin, J. Ye and Y. Chao, *RSC Adv.*, 8 (2018) 2552.
20. Q.H. Wang, Y.C. Ma, Y.L. Wang, H.B. Bao, A.Q. Li, P. Xu, X.M. Li and W.J. Yang, *Nanotechnology*, 31 (2020) 055601.
21. M. Bahrami, G. Taton, V. Conedera, L. Salvagnac, C. Tenailleau, P. Alphonse and C. Rossi, *Propell. Explos. Pyrot.*, 39 (2014) 365.

22. A.H. Kinsey, K. Slusarski, E. Krumheuer and T.P. Weihs, *J. Mater. Sci.*, 52 (2017) 11077.
23. J. Song, T. Guo, M. Yao, W. Ding, X. Zhang, F. Bei, J. Tang, J. Huang and Z. Yu, *RSC Adv.*, 9 (2019) 41319.
24. J. Wang, Z. Qiao, Y. Yang, J. Shen, Z. Long, Z. Li, X. Cui and G. Yang, *Chemistry*, 22 (2016) 279.
25. Y.J. Yin and X.M. Li, *J. Mater. Eng. Perform.*, 29 (2020) 1375.
26. Y.J. Yin and X.M. Li, *Vacuum*, 163 (2019) 216.
27. Q. Wang, B. Xing, X. Guo, H. Bao, Y. Wang, A. Li, P. Xu and X. Li, *Vacuum*, 167 (2019) 244.
28. Q. Wang, S. Yang, H. Bao, Q. Wang, X. Li and W. Yang, *Vacuum*, 169 (2019) 108881.
29. X. Zhou, D.G. Xu, Q.B. Zhang, J. Lu and K.L. Zhang, *ACS Appl. Mater. Interfaces*, 5 (2013) 7641.
30. P. Zhu, R. Shen, Y. Ye, S. Fu and D. Li, *J. Appl. Phys.*, 113 (2013) 184505.
31. F. Severac, P. Alphonse, A. Esteve, A. Bancaud and C. Rossi, *Adv. Funct. Mater.*, 22 (2012) 323.
32. Y. Yang, D. Xu and K. Zhang, *J. Mater. Sci.*, 47 (2012) 1296.
33. Y. Ohkura, S.Y. Liu, P.M. Rao and X. Zheng, *P. Combust. Inst.*, 33 (2011) 1909.
34. P. Sarkar and P.S. Nicholson, *J. Am. Ceram. Soc.*, 78 (1995) 3165.
35. K.T. Sullivan, M.A. Worsley, J.D. Kuntz and A.E. Gash, *Combust. Flame*, 159 (2012) 2210.
36. D.X. Zhang and X.M. Li, *J. Phys. Chem. A*, 119 (2015) 4688.
37. B. Choudhary, S. Anwar, L. Besra and S. Anwar, *Int. J. Appl. Ceram. Technol.*, 16 (2019) 1022.
38. N. Koura, T. Tsukamoto, H. Shoji and T. Hotta, *Jpn. J. Appl. Phys.*, 34 (1995) 1643.
39. E. Khoo, P.S. Lee and J. Ma, *J. Eur. Ceram. Soc.*, 30 (2010) 1139.
40. B. Qian, H. Dai, S.F. Tang and Z.W. Song, *Optik*, 178 (2019) 128.
41. A.V. Alekseev and P.V. Yakimovich, *Meas. Tech.*, 62 (2019) 741.
42. Q. Yin, Y. Zhu, S. Ju, W. Liao and Y. Yang, *Res. Chem. Intermed.*, 42 (2016) 4985.
43. M. Nasiri-Majd, M.A. Taher and H. Fazelirad, *Ionics*, 22 (2016) 289.
44. N.K. Temel and R. Gurkan, *J. Anal. Chem.*, 74 (2019) 1174.